

Spectral weight redistribution in strongly correlated bosons in optical lattices

C. Menotti^{1,2} and N. Trivedi³

¹ *ICFO - Institut de Ciències Fotoniques, Mediterranean Technology Park, E-08860 Castelldefels (Barcelona), Spain*

² *CNR-INFM-BEC and Dipartimento di Fisica, Università di Trento, I-38050 Povo (Trento), Italy*

³ *Department of Physics, The Ohio State University, Columbus, Ohio 43210, USA*

We calculate the single-particle spectral function for the one-band Bose-Hubbard model within the random phase approximation (RPA). In the strongly correlated superfluid, in addition to the gapless phonon excitations, we find extra gapped modes which become particularly relevant near the superfluid-Mott quantum phase transition (QPT). The strength in one of the gapped modes, a precursor of the Mott phase, grows as the QPT is approached and evolves into a hole (particle) excitation in the Mott insulator depending on whether the chemical potential μ is above (below) the tip of the lobe. The sound velocity c of the Goldstone modes remains finite when the transition is approached at a constant density, otherwise, it vanishes at the transition. It agrees well with Bogoliubov theory except close to the transition. We also calculate the spatial correlations for bosons in an inhomogeneous trapping potential creating alternating shells of Mott insulator and superfluid. Finally, we discuss the capability of the RPA approximation to correctly account for quantum fluctuations in the vicinity of the QPT.

PACS numbers: 05.30.Jp, 03.75.Lm, 71.45.Gm, 37.10.Jk

I. INTRODUCTION

Optical lattices have made it possible to explore the properties of ultracold dilute atoms in a new regime of strong correlations^{1,2,3}. By tuning the strength of the laser field, the effective interactions between atoms can be tuned to become stronger than their kinetic energy. For Bose systems, such a competition between kinetic t and interaction energy U drives a quantum phase transition^{4,5} from a kinetic energy dominated superfluid (SF) phase to an interaction dominated Mott insulating (MI) phase. The Bose Hubbard model (BHM) captures the essential physics of this problem⁴, provided the interactions between the bosons are smaller than interband energies and the problem can be treated in the single band approximation. While the BHM was proposed much before optical lattice experiments became available, a direct experimental realization was missing. In condensed matter systems, Josephson junction arrays⁶, ⁴He in vycor and aerogels⁷, vortices in superconductors⁸ and quantum magnets⁹ can be modeled by the BHM, but the actual systems have additional complications of disorder or longer range interactions which make the comparisons between theory and experiment difficult.

One of the main advantages of the cold atom systems is that they are clean and much more tunable: the density of bosons, their effective interaction, the tunneling amplitude between the wells, the number of lattice sites, the shape of the trapping potential and aspect ratios can all be varied rather easily, making it possible to study the effects of inhomogeneity and dimensionality. In addition, it is possible to add random potentials to study the effects of disorder. This sets the optical lattice systems apart as a useful testing ground for theoretical ideas in the area of strongly interacting bosons and fermions. This model has also provided tremendous impetus for the development of new measurement techniques to address

questions about the nature of the excitations especially near the transition^{10,11,12,13,14,15,16,17,18}. The recent experiments on the dynamics^{19,20} have given a window into the different time scales operating within the different phases and around the quantum phase transitions.

The paper is organised as follows: In Sect. II, we present the Bose-Hubbard model and state our main results. In Sect. III, we discuss the nature of the spectral function calculated within the RPA formalism as it evolves from the SF to the MI phase by decreasing t/U . The sound velocity in the SF phase and its comparison with Bogoliubov theory is contained in Sect. IV. The momentum distribution and the spatial correlations are calculated in Sect. V. The RPA formalism is generalized to a spatially inhomogeneous trapping potential in Sect. VI. We conclude in Sect. VII with some remarks about the comparison between RPA and mean field theory. There are three appendices that give the details of the calculations of the Green function within RPA (App. A), the Bogoliubov calculation for the Bose-Hubbard model (App. B), and the momentum distribution function within RPA in the Mott regime (App. C).

II. MODEL AND MAIN RESULTS

The Bose-Hubbard Hamiltonian is defined as

$$H = -\frac{t}{2z} \sum_{\langle ij \rangle} (a_i^\dagger a_j + a_i a_j^\dagger) + \frac{U}{2} \sum_i n_i(n_i - 1) - \mu \sum_i n_i, \quad (1)$$

where a_i and a_i^\dagger are bosonic annihilation and creation operators respectively and $n_i = a_i^\dagger a_i$ is the density operator. The parameter U describes the on-site repulsive interaction between bosons, t is the tunneling parameter between nearest neighbors as indicated by the symbol

$\langle ij \rangle$, μ is the chemical potential that fixes the number of particles and $z = 2D$ is the coordination number in D dimensions. This Hamiltonian shows a quantum phase transition (QPT) from the SF to the MI phase as a function of t/U . The theoretical approaches used to investigate this Hamiltonian include mean field theory²¹, perturbation theory²², variational methods²³ and quantum Monte Carlo simulations^{24,25}.

In this paper, we use a Green's function formalism to investigate the excitations and correlations in the BHM. We start from the mean-field (MF) ground state which is essentially a product of single site states and go beyond it by including inter-well coupling within a random phase approximation (RPA)^{26,27}.

Our main results are as follows:

(1) In the weakly interacting SF ($t/U \approx 100$) the gapless phonons of the SF, or the Goldstone modes arising due to the broken gauge symmetry, exhaust the sum rule on the total spectral weight, as expected. For $t/U \approx 10$ there are already small deviations from Bogoliubov theory and new gapped modes appear in the SF phase. These gapped modes pick up strength as $t/U \approx 1$. The sum rule is now satisfied only upon including *both* phonon and gapped modes.

(2) At the transition, we observe the progression of one of the phonon modes in the SF into a gapped mode in the MI (the one which is gapless at the QPT). The second gapped mode in the MI instead arises from one of the gapped modes in the SF. Such gapped modes in the SF have been reported previously using several theoretical methods^{14,15,16,17}. We argue that these additional gapped modes are a distinctive signature of a strongly correlated SF in proximity to a MI in an optical lattice. They indicate the redistribution of spectral weight from the coherent phonon modes into incoherent excitations, and are a precursor of the MI beyond the QPT.

(3) We calculate the sound velocity in the RPA formalism and show that it agrees with $c = 1/\sqrt{\kappa m^*}$ calculated independently from the mean-field effective mass and compressibility. In a wide range of parameters, except very close to the SF-MI phase transition, the above sound velocity compares well with the predictions of Bogoliubov theory.

(4) We exploit a special feature of superfluids that allows us to extract the condensate fraction n_0 from the strength of the phonon modes in the spectral function.

(5) We calculate the spatial correlations in the case where an inhomogeneous confining potential is superimposed on the optical lattice. The response to a perturbation is strongly influenced by the presence of alternating shells of Mott insulator and superfluid regions.

III. FORMALISM: RPA APPROXIMATION, SPECTRAL FUNCTION, AND EXCITATIONS

We start with the mean-field approximation in real space²¹ obtained by giving the annihilation and creation

operators an expectation value defined by $\langle a \rangle = \langle a^\dagger \rangle = \varphi$. The order parameter φ identifies the nature of the system: it is non-zero in the SF phase and vanishes in the insulating phase. Substituting $a = \varphi + \tilde{a}$, $a^\dagger = \varphi + \tilde{a}^\dagger$, in Eq. (1), where \tilde{a} and \tilde{a}^\dagger are the fluctuations of the Bose field around the mean field value, the Hamiltonian H can be rewritten as a sum of on-site Hamiltonians

$$H_i^{MF} = \frac{U}{2} n_i(n_i - 1) - \mu n_i - t\varphi(a_i^\dagger + a_i) + t\varphi^2, \quad (2)$$

which include the tunneling at the mean field level through the order parameter φ . In the MF approximation, we neglect the non-local inter-well hopping term $-(t/2z) \sum_{\langle ij \rangle} (\tilde{a}_i^\dagger \tilde{a}_j + \tilde{a}_i \tilde{a}_j^\dagger)$, which we will later treat in RPA.

The H_i^{MF} can be diagonalized numerically, leading to a set of on-site eigenstates such that $H_i|i\alpha\rangle = \epsilon_\alpha|i\alpha\rangle$. In the Mott limit the eigenstates $|i\alpha\rangle$ are number states, while in the SF regime they are coherent superpositions of several number states, allowing the order parameter to be different from zero. The MF ground state solution is given by the product state $|\Phi\rangle = \prod_i |i, 0\rangle$, equivalent to the one obtained in the Gutzwiller Ansatz, where $|i, 0\rangle$ is the ground state of H_i^{MF} .

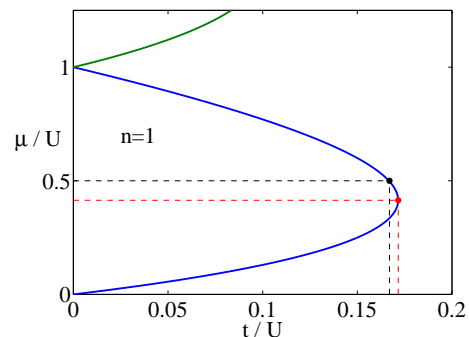


FIG. 1: (Color online) Mean field phase diagram in the μ/U vs. t/U plane. The blue line shows the Mott insulating lobe at density $n = 1$. On this diagram, we indicate two points where the QPT happens, that we are going to discuss in this paper: a generic one at $\mu/U = 0.5$ and $t/U \approx 0.167$ (black) and the tip of the lobe at $\mu/U = \sqrt{2} - 1$ and $t/U \approx 0.1716$ (red) where the QPT takes place at constant density.

Within the mean field approximation, the state of the system is described by a product state over the different wells, neglecting all inter-well correlations. However, even in the MI, correlations between neighboring wells do not vanish; in fact they get large as t/U is increased from the Mott side, ultimately diverging at the transition. Experimental evidence of these correlations is found in the interference picture of an atomic cloud released from a 3D optical lattice, the visibility of which does not suddenly

vanish at the phase transition^{28,29,30,31,32}. These important features are captured by the RPA performed on the non-local tunneling terms of the BHM. At the end of this paper, we discuss the limitations of the RPA method and how it compares with the mean-field approximation.

To go beyond the mean-field approximation, we treat the inter-well hopping term within RPA, as described in App. A^{26,27}. This method allows us to compute the Green's function $G(\mathbf{q}, \omega) = \langle \langle a_{\mathbf{q}}^\dagger; a_{\mathbf{q}} \rangle \rangle_\omega$, defined in Eqs. (A4, A6), and from that, the spectral function $\mathcal{A}(\mathbf{q}, \omega) = -(1/\pi) \text{Im} G(\mathbf{q}, \omega)$.

Due to the commutation relations of the bosonic destruction and creation operators, the spectral function always satisfies the sum rule

$$\int_{-\infty}^{\infty} \mathcal{A}(\mathbf{q}, \omega) d\omega = 1. \quad (3)$$

From the spectral function, one can extract the excitation spectrum, the strength of the excitation modes, and the related density of states

$$\text{DOS}(\omega) = \int \mathcal{A}(\mathbf{q}, \omega) d\mathbf{q}. \quad (4)$$

Moreover, the spectral function is an essential ingredient to compute the momentum distribution

$$n(\mathbf{q}) = \langle a_{\mathbf{q}}^\dagger a_{\mathbf{q}} \rangle = \int_{-\infty}^0 \mathcal{A}(\mathbf{q}, \omega) d\omega \quad (5)$$

and the single particle density matrix given by the Fourier transform of the momentum distribution in real space

$$\rho(\mathbf{r}, \mathbf{r}') = \langle a_{\mathbf{r}}^\dagger a_{\mathbf{r}'} \rangle = \frac{1}{N} \sum_{\mathbf{q}} e^{i\mathbf{q} \cdot (\mathbf{r} - \mathbf{r}')} n(\mathbf{q}), \quad (6)$$

where N indicates the number of lattice wells. The long distance behavior of $\rho(\mathbf{r}, \mathbf{r}')$ as a function of the relative distance approaches the condensate density n_0 which is non zero in a SF and vanishes in the MI. In the following we will calculate and discuss all these quantities.

A fundamental implication of broken symmetry for bosonic systems is that the Goldstone modes are directly reflected in the single particle spectrum. In other words, phonons which are related to modes of density-density fluctuations (or two-particle Green function) also show up as the poles in the single particle Green function³³. We study the behavior of the poles of the Green's function, their strength, momentum and frequency dependence, to extract information about the excitations of the system. In the two extreme limits of deep MI and weakly interacting (Bogoliubov) SF, the Green's function can be calculated analytically and from it, the excitations frequencies and the momentum distribution $n(\mathbf{q})$.

A. Deep Mott regime

In the deep Mott regime (zero tunneling), for $U(n-1) < \mu < Un$, one finds

$$G_{MI}(\mathbf{q}, \omega) = \frac{1}{2\pi} \left[\frac{n+1}{\omega - (Un - \mu)} - \frac{n}{\omega - (U(n-1) - \mu)} \right] \quad (7)$$

$$\omega_{MI}(\mathbf{q}) = \begin{cases} Un - \mu > 0 \\ U(n-1) - \mu < 0 \end{cases} \quad (8)$$

$$n_{MI}(\mathbf{q}) = n, \quad \forall \mathbf{q}, \quad (9)$$

where n is the atomic occupation at each lattice site. The spectral function consists of two δ -functions, one at positive energy $Un - \mu$ (relative to the chemical potential) required to add a particle and one at negative energy $U(n-1) - \mu$, required to remove a particle or add a hole to the MI, as seen in Eq. (8). The spectral function $\mathcal{A}(\mathbf{q}, \omega)$ obtained using expression (7) trivially satisfies the sum rule in Eq. (3). The momentum distribution, as defined in Eqs. (5, 9), is completely flat, corresponding to vanishing site-to-site correlations, and normalized to the total number of atoms in the lattice (n times the number of sites). Correspondingly, the single particle density matrix (6), given by the Fourier transform of the momentum distribution, shows strictly on-site correlations.

B. Weakly interacting regime

In the weakly interacting SF regime³⁴, we have

$$G_{BG}(\mathbf{q}, \omega) = \frac{1}{2\pi} \left[\frac{|u_{\mathbf{q}}|^2}{\omega - \omega_{\mathbf{q}}} - \frac{|v_{-\mathbf{q}}|^2}{\omega + \omega_{-\mathbf{q}}} \right], \quad (10)$$

$$\omega_{BG}(\mathbf{q}) = \pm \omega_{\pm \mathbf{q}}, \quad (11)$$

$$n_{BG}(\mathbf{q}) = n_0 \delta_{\mathbf{q}, 0} + |v_{-\mathbf{q}}|^2, \quad (12)$$

where $u_{\mathbf{q}}$ and $v_{\mathbf{q}}$ are the Bogoliubov amplitudes, $\omega_{\mathbf{q}}$ is the Bogoliubov frequency at momentum \mathbf{q} (see App. B for details), and n_0 the condensate density. In the weakly interacting SF regime, the sum rule in Eq. (3) is constrained by the Bogoliubov normalization condition $|u_{\mathbf{q}}|^2 - |v_{-\mathbf{q}}|^2 = 1$. The excitation energies are given by symmetric poles at positive and negative frequencies corresponding to the energies of the Bogoliubov spectrum, highlighting in particular phononic excitations at low momentum.

The momentum distribution, given by integrating the spectral function over negative energies, has a singular contribution from the condensate at zero momentum. The integral over all momenta different from zero gives the number of non condensed atoms, contributing the depletion from the condensate. In the regime where Bogoliubov theory is valid, the depletion is negligible compared to the atoms in the condensate.

C. Progression from SF to MI

The RPA formalism allows us to calculate the spectral function with special emphasis on the strong correlation region near the QPT. In the deep SF, we find phonon collective modes reflected in the single particle spectrum. As t/U is decreased, the spectral weight is redistributed over a multi-mode structure composed by coherent phonon excitations and gapped single-particle excitations. When entering the MI phase at the QPT, the spectral weight reorganises and is shared by only two gapped modes, describing single particle excitations, one at positive and one at negative energy. In the following, we will discuss this behaviour more in detail.

We use the position of the poles of the Green's function to determine the following results about the excitations of the system in the different regimes:

(i) For a large number of particles per site (≈ 100) and weak interactions ($t/U \approx 100$), we exactly recover the Bogoliubov results. We point out that being able to describe the weakly interacting regime starting from the BHM is not a trivial result, because of the large number of basis states required (almost 150 states per site).

(ii) By increasing the interactions and decreasing the number of particles per site, we observe small deviations between the spectrum obtained by RPA and the Bogoliubov theory: additional modes appear at higher frequencies, as shown in Fig. 2(a) for $t/U = 10$, in contrast with Bogoliubov theory which predicts a single excitation mode. While there are also differences in the dispersion of the sound modes at large momenta, we find in general that the Bogoliubov prediction turns out to be quite accurate in describing the low- q part of the spectrum and the sound velocity, even in the case of strong interactions (see Sect. IV).

(iii) As t/U becomes of order unity and the effect of strong correlations grows, additional gapped modes in the SF phase are clearly visible and grow in strength as seen in Fig. 2(b). The phonon modes are not sufficient to exhaust the sum rule in Eq. (3). In a strongly interacting SF (e.g for $t/U < 0.25$, as shown in Fig. 2(c)), many modes (in the cases we have considered, up to four at positive and four at negative energy) have to be included in order to exhaust the sum rule in Eq. (3). In the particular case of $\mu/U = 0.5$ and $t/U = 0.25$, the full dispersion of the modes is shown in Fig. 3(b).

(iv) In the MI, only two excitation modes exist, as shown in Figs. 2(d) and 3(a). The mode at positive and the one at negative energy correspond respectively to the energy needed to create a particle or a hole in the system. For any given t/U , the difference of the excitation energies at $q = 0$ exactly coincides to the width of the mean-field Mott lobe at the same t/U .

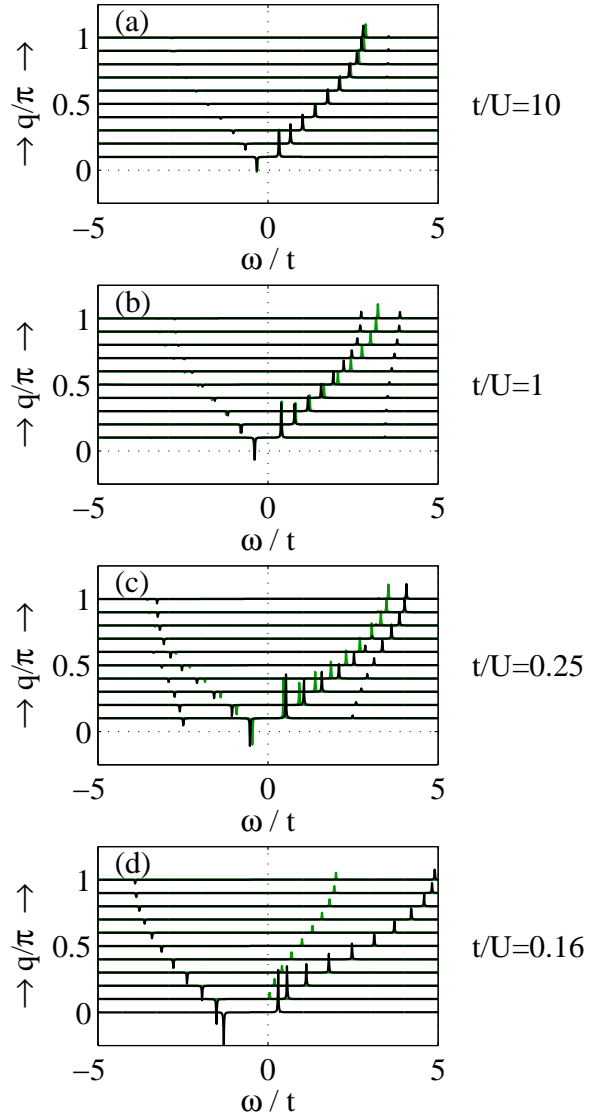


FIG. 2: (Color online) Spectral function $\mathcal{A}(q, \omega)$ as a function of ω for various q . Results obtained by RPA (black) and Bogoliubov theory (green). (a) Weakly interacting SF: $t/U = 10$ with ≈ 10 bosons per site; the RPA calculation agrees extremely well with the Bogoliubov theory; notice indications of additional modes at higher ω . (b) $t/U = 1$ with ≈ 1.8 bosons per site. (c) Strongly interacting SF: $t/U = 0.25$ with ≈ 1.1 bosons per site; stronger deviations from Bogoliubov theory are present especially at larger q . Additional modes are clearly visible in the spectrum. (d) Mott insulating phase for $t/U = 0.16$ and 1 boson per site. In all those figures $\mu/U = 0.5$.

D. Strengths of the spectral function

The progression of the modes from the strongly correlated SF into the MI is better understood by calculating the strengths of the excitations S_i , defined as follows:

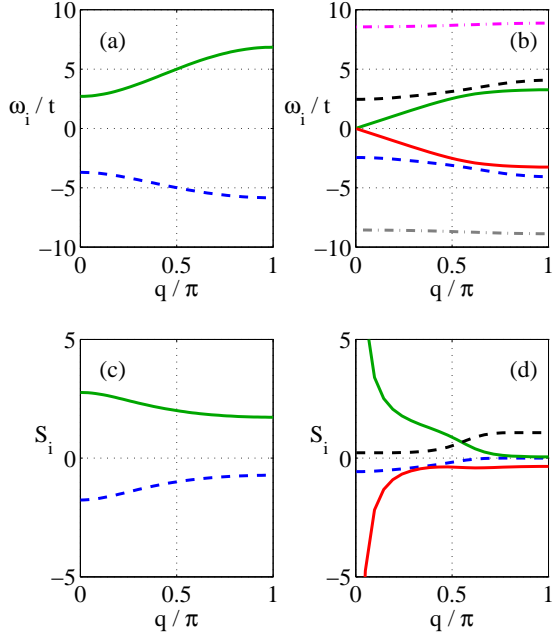


FIG. 3: (Color online) Dispersion (a,b) and strength (c,d) of excitation modes at $\mu/U = 0.5$: (a) and (c) are in the Mott regime $t/U = 0.1$; (b) and (d) are in the SF regime $t/U = 0.25$. For clarity, in (b) the 4th pair of resonances at $\omega \approx \pm 18.4$ is not shown and in (d) only the strength of the 4 modes at lower energy is shown. Note that modes at positive (negative) energy have positive (negative) strength.

$$\mathcal{A}(\mathbf{q}, \omega) = \sum_i S_i \delta(\omega - \omega_i). \quad (13)$$

Numerically, a small but finite imaginary part of the energy regularizes the spectral function and provides an accurate fitting procedure to determine the position of the poles and their strength. We checked that the sum rule in Eq. (3), which using Eq. (13) implies $\sum_i S_i = 1$, was found to be satisfied to better than few parts in 10^{-5} for all t/U . We are therefore confident that we have identified all the excitations which contribute in a non-negligible way to the spectrum.

In Figs. 4,5, we plot the position of the resonances and their strengths for a fixed value of $q = \pi/50$, varying the parameter t/U across the phase transition for fixed chemical potential. As explained above, the many-mode spectrum in the SF phase evolves into the two-mode excitation spectrum in the MI.

The transition from the MI to the SF phase occurs when one of the two Mott branches becomes gapless (see Fig. 4(a)). This is the particle (hole) gapped mode in the MI depending on whether the chemical potential μ is

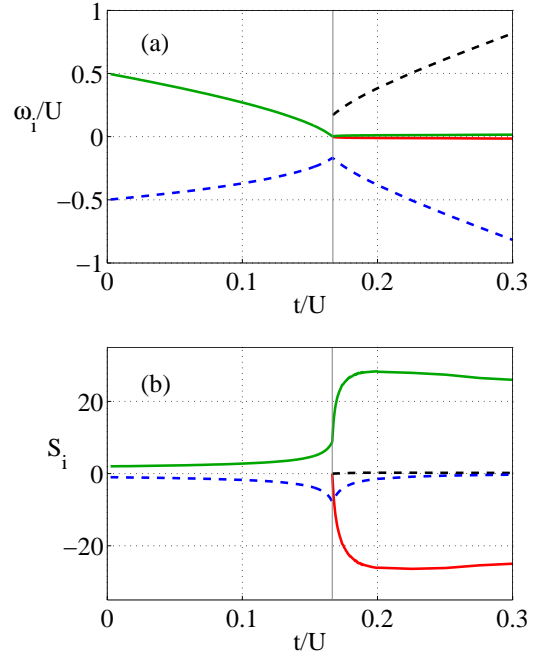


FIG. 4: (Color online) Energy (a) and strength (b) of the modes at low $q = \pi/50$ as a function of t/U for $\mu/U = 0.5$. Notice the presence of both phonons and gapped modes in the strongly interacting SF and their evolution into two gapped modes into the MI. One of the gapped modes in the MI evolves from the phonon mode in the SF and the other one from a gapped mode in the SF. The thin vertical line at $t/U \approx 0.167$ indicates the QPT.

above (below) the tip of the lobe. This Mott branch evolves into the phononic mode at positive (negative) energy, while the other phononic mode arises at zero strength without having a precursor in the Mott phase. The second Mott branch evolves into a gapped superfluid mode, and symmetrical in energy a second superfluid gapped mode arises with zero strength without having a precursor in the Mott phase (see Fig. 4(b)).

The behavior at the tip of the lobe is quite interesting. In that case both Mott gapped modes become simultaneously gapless at the QPT (see Fig. 5(a)). From them the lowest four modes in the SF arise, two of them becoming phononic modes and two of them becoming gapped modes when moving away from the transition. However, within our approach, we find a similar behavior to the one described above, namely that one of the Mott modes evolves into a SF phononic mode, while the second one evolves into a SF gapped mode (see Figs. 5(b)).

A similar result was found by Huber and collaborators¹⁷ using an effective 3-state approximation and mapping onto a spin-1 Hamiltonian. They further suggested that measurements of the dynamical structure factor using Bragg spectroscopy and lattice modulations could be an effective way to investigate the different modes.

The problem was also investigated by Sengupta and Dupuis¹⁴ in the strong coupling regime by deriving an

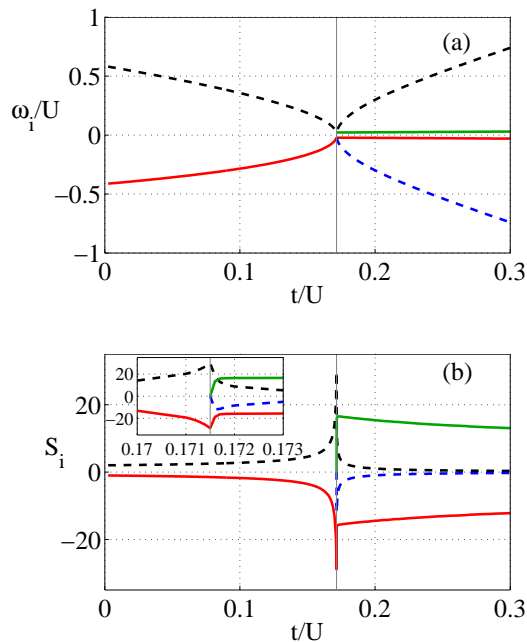


FIG. 5: (Color online) Energy (a) and strength (b) of the modes at low $q = \pi/50$ as a function of t/U at $\mu/U = \sqrt{2} - 1$ corresponding to the tip of the lobe. The frequency of the lowest four modes (two phononic and two gapped) in the SF vanish at the QPT. The thin vertical line at $t/U \approx 0.1716$ indicates the QPT. In the inset, the zoom around the QPT of panel (b) is shown.

effective action using Hubbard Stratonovich transformations. By expanding the action to quadratic order in the fluctuations they found gapped excitations in the MI and gapless Goldstone modes in the SF. They found two additional gapped modes in the SF, which present a similar behavior to the one discussed in this paper.

E. Density of states

A further quantity that one can use to characterise the excitations of the system is the density of states defined in Eq. (4)^{14,16}. We calculate it across the QPT for a 1D system³⁵, as shown in Fig. 6. In Fig. 6(a) one can recognize the multi-mode structure of a strongly correlated SF through a clearly enhanced DOS in the energy range of the corresponding excitation branch. In particular, we can see here two phononic branches and two gapped ones. When approaching the QPT ($t/U = 0.17$ and Fig. 6(b)), we encounter a similar structure, where the width of the gapped branch at negative energy is increased, while the gapped branch at positive energy is not visible on the scale of this picture (although existing), since its strength goes to zero at the QPT. As expected, in the Mott regime, the DOS is different from zero only in the energy range of the two gapped excitation branches, one at negative and one at positive energy (Figs. 6(c,d)).

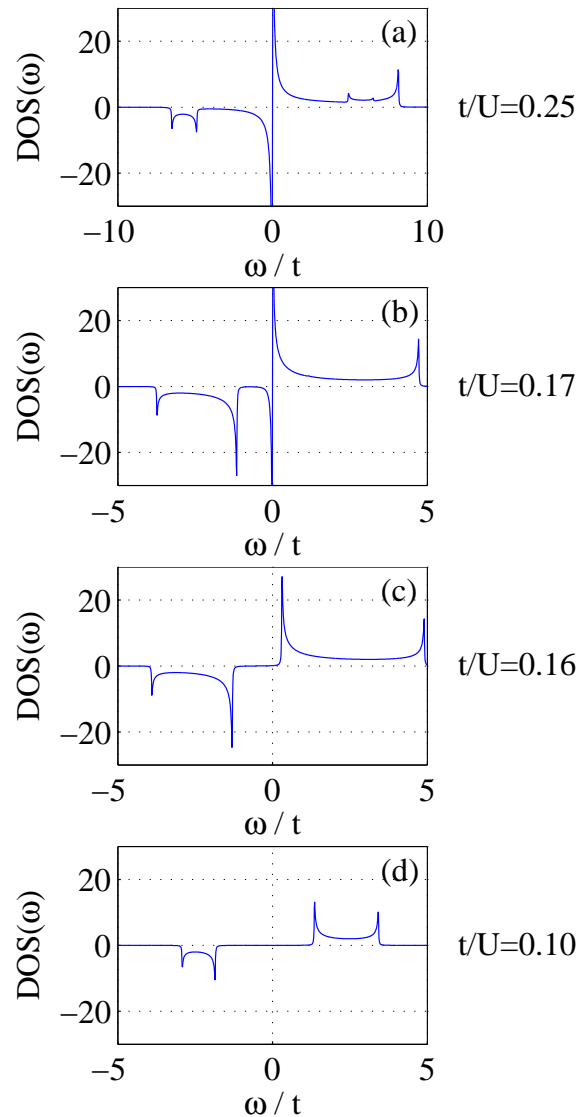


FIG. 6: Density of states for several values of t/U . (a) $t/U = 0.25$, SF regime; (b) $t/U = 0.17$, SF regime, very close to the QPT; (c) $t/U = 0.16$ MI regime, very close to the QPT; (d) $t/U = 0.1$ MI regime. All those results are for $\mu/U = 0.5$.

As observed in Fig. 6(c), the branch at positive energy extends almost to $\omega = 0$, indicating the disappearance of the gap at the QPT.

IV. SOUND VELOCITY

The presence of phononic modes in the excitation spectrum is an important signature of superfluidity. These modes disappear in the Mott phase, where sound cannot propagate because of a gap in the spectrum. In this section, we discuss the evolution of the sound velocity in the

strongly correlated SF phase as the SF-MI transition is approached.

The sound velocity is related to the compressibility κ and the effective mass m^* ^{36,37,38} through the relation

$$c = \frac{1}{\sqrt{\kappa m^*}} = \sqrt{\frac{\rho_s}{\rho \kappa}} m, \quad (14)$$

where $\kappa^{-1} = \rho(\partial\mu/\partial\rho)$ and the SF fraction $\rho_s/\rho = m/m^*$. We calculate the sound velocity c from the slope of the gapless mode in the RPA spectrum

$$\lim_{|\mathbf{q}| \rightarrow 0} \omega(\mathbf{q}) = c|\mathbf{q}|, \quad (15)$$

and compare it with the one obtained with the compressibility relation in Eq. (14). We find perfect agreement between the values for the sound velocity extracted by the two different methods. It is important to note that the method using the compressibility relation in Eq. (14) only requires the knowledge of the mean-field solution, which provides the equation of state $\mu(\rho)$ and the SF density $\rho_s = |\varphi|^2$.

We find that when the SF-MI transition, tuned by t/U and μ/U , is approached at a generic point away from the tip of the lobe, the sound velocity vanishes, as shown in Fig. 7(a). This is due to the fact that at the transition the compressibility remains finite, but the SF density vanishes. Instead, the tip of the lobe where the phase transition happens at constant density and $\partial\rho/\partial\mu = 0$ is a special point: there, a perfect compensation between the divergent inverse compressibility and the vanishing SF density takes place, which results in a finite sound velocity as seen in Fig. 7(b).

We complete our analysis by comparing the sound velocity calculated above with the results of Bogoliubov theory, which for a tunneling parameter t , on-site interaction U and coordination number z , predicts the value

$$c_{BG} = \sqrt{\frac{2t}{z} U |\varphi|^2}, \quad (16)$$

as explained in detail in App. B. The Bogoliubov predictions are remarkably good in a wide range of parameters and fail only in the close proximity of the phase transition (see thin lines in Fig. 7), since Bogoliubov theory does not account correctly for the vanishing of the order parameter at that point.

V. MOMENTUM DISTRIBUTION AND SPATIAL CORRELATIONS

From Eq. (5), the momentum distribution $n(\mathbf{q})$ is obtained by integrating the spectral function over negative

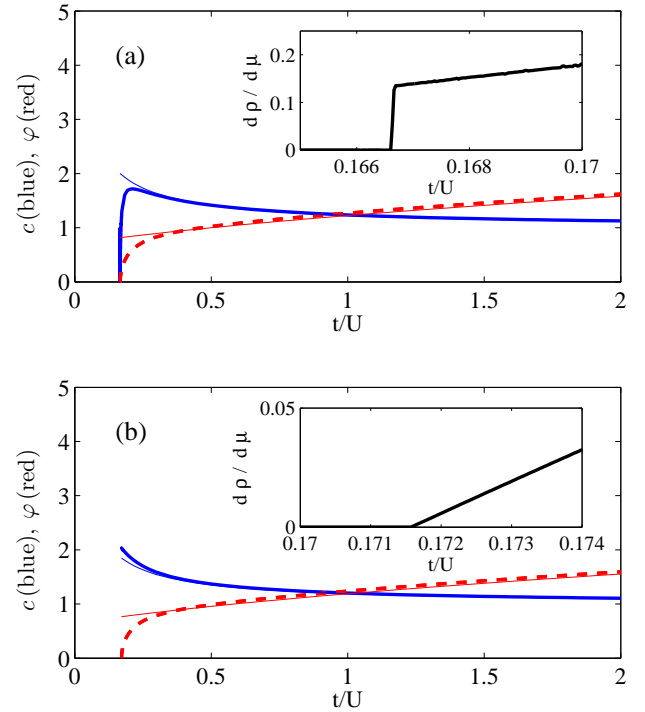


FIG. 7: (Color online) Sound velocity c (blue full line) extracted from the slope of the dispersion of the phonon modes and from Eq. 14; order parameter φ (red dashed line). Also shown for comparison are the sound velocity and the order parameter obtained from Bogoliubov theory (thin lines). In the inset $d\rho/d\mu$ is shown. (a) $\mu/U = 0.5$; (b) $\mu/U = \sqrt{2} - 1$, corresponding to the tip of the lobe.

energies. It is a quantity of primary importance in cold atom experiments, as it is directly accessible by imaging the cloud after expansion^{3,31,32}. We have considered a two-dimensional system, which allows for the existence of Bose-Einstein condensation with long range order in the SF regime.

The 2D momentum distribution is shown in Fig. 8 for different values of the parameter t/U . We have checked that we can reproduce the momentum distribution in the two extreme cases of deep MI (see Eq. (9)) and weakly interacting SF (see Eq. (12)).

In the Mott phase with non vanishing tunneling, we find that the momentum distribution presents a modulation showing up as interference peaks in the expansion pictures^{29,31}. When the QPT is reached, a strong peak develops at $q = 0$ corresponding to the condensate. However, in a SF close to the phase transition the background momentum distribution (at $q \neq 0$) is large indicating a strong depletion from the condensate due to interactions.

The momentum distribution obtained with the RPA method happens to be not correctly normalized to the total number of atoms. We attribute this feature to the

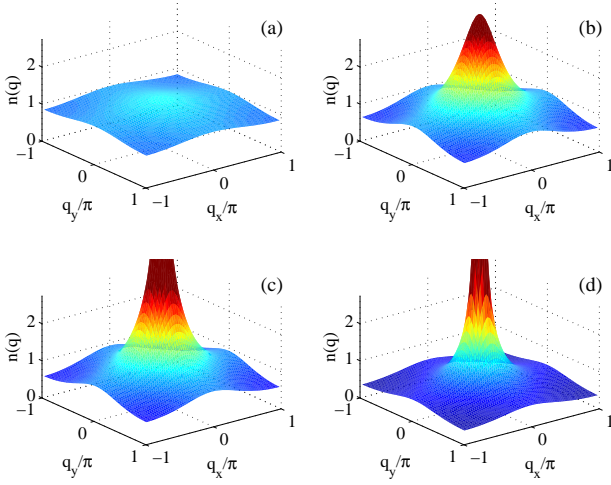


FIG. 8: (Color online) Momentum distribution $n(\mathbf{q})$ for a 2D system for $\mu/U = 0.5$ and (a) $t/U = 0.05$ deep in the MI; (b) $t/U = 0.15$ in the MI but closer to the QPT; (c) $t/U = 0.175$ in the SF phase close to the QPT; (d) $t/U = 0.25$ in the SF phase but further from the QPT.

fact that fluctuations are not self-consistently included in the ground state (see discussion in App. C).

Starting from the momentum distribution, one can obtain the single particle density matrix $\rho(\mathbf{r}, \mathbf{r}')$, which contains direct information about the spatial correlations present in the system. In the SF phase, the system is characterized by off-diagonal long range order, and at long distances, the single particle density matrix approaches a constant value equal to the square of the order parameter, or the condensate density n_0

$$\rho(\mathbf{r}, \mathbf{r}') \equiv \langle a^\dagger(\mathbf{r})a(0) \rangle \rightarrow \varphi^2 = n_0, \quad (17)$$

which is non-zero in a SF. This quantity is linked through Fourier transform to the δ -function at $\mathbf{q} = 0$ which appears in the momentum distribution.

The single particle density matrix in Fig. 9 shows a marked transition from the MI phase to the SF, and corresponds to a change from an exponential decay of the correlations to a (quasi) long range order. In the MI, the single particle density matrix shows that the correlations decay over a finite length scale, which decreases by decreasing the tunneling and moving deeper into the Mott lobe. From those results, we have direct access to the length scale of the correlations in the insulating regime.

The condensate fraction can be in principle extracted from the momentum distribution, by subtracting the depletion $\sum_{\mathbf{q} \neq 0} n(\mathbf{q})$ from the total density n , or equivalently by looking at the asymptotic value at large distances of the single-particle density matrix $\rho(\mathbf{r}, \mathbf{r}')$. However, unfortunately we find that the present application of RPA gives a violation of the total density sum rule

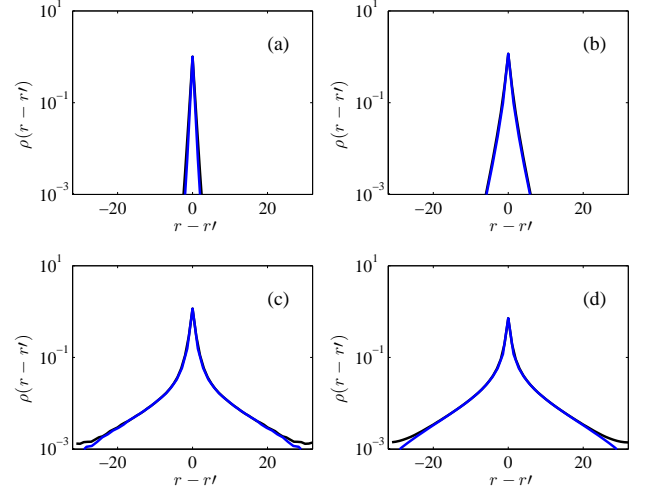


FIG. 9: (Color online) Density matrix $\rho(r, r')$ as a function of the relative distance $r - r'$ for a 2D system (black line for a cut in the center of the trap and blue line along the diagonal). (a) $t/U = 0.05$ deep in the MI showing only nearest neighbor correlations; (b) $t/U = 0.15$ in the MI but closer to the QPT showing an increase in the scale of the short range correlations; (c) $t/U = 0.175$ in the SF phase close to the QPT showing long range order; (d) $t/U = 0.25$ in the SF phase but further from the QPT. Note that the asymptotic value for large $r - r'$ has been subtracted.

and $\sum_{\mathbf{q} \neq 0} n(\mathbf{q}) > n$ (see also discussion in App. C), so that neither the momentum distribution nor the single-particle density matrix turn out to be useful quantities to extract the condensate density. This problem arises because within the present theoretical description, we have not included the feedback of the collective modes and other excitations into the mean field ground state. Possible solutions to this problems will be topic of further research³⁹.

However, our analysis of the excitation modes and their strength allows us to extract the condensate density n_0 directly, using our knowledge of the sound velocity (from the slope of the phononic mode at small momenta), combined with the knowledge of the strengths of the spectral function and the compressibility. Starting from the relation

$$\mathcal{A}(q, \omega) = \frac{n_0}{\rho_s} m c^2 \delta(\omega^2 - c^2 q^2), \quad (18)$$

and assuming that the condensate and SF densities are equal (at least within mean field theory), we get

$$n_0 = \frac{(2qS_{ph})^2}{m^* d \mu / d \rho} = \frac{(4\pi q S_{ph})^2 t}{d \mu / d \rho}. \quad (19)$$

where S_{ph} is the strength of the phononic modes. We have used $t = \hbar^2 / (m^* d^2)$ (with $\hbar = 1/2\pi$ and lattice spacing $d = 1$) to relate the effective mass and the tunneling parameter in the BHM.

The limiting behavior of the RHS of Eq. (19) for very small q approaches the condensate density which coincides with the predictions of mean-field theory ($|\varphi|^2$), as shown in Fig. 10.

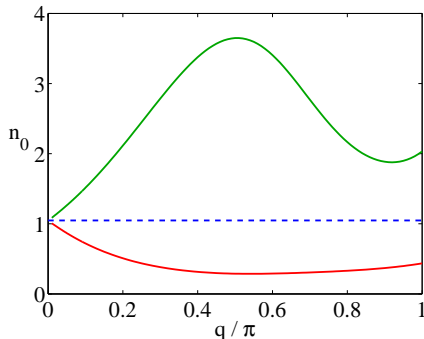


FIG. 10: (Color online) Condensate fraction obtained from the strength of the poles of the spectral function, as in Eq. (19), for the phonon mode at positive (upper green line) and negative (lower red line) frequency. As $q \rightarrow 0$ both functions approach the condensate fraction n_0 obtained with MFT (dashed blue line). In this figure $\mu/U = 0.5$ and $t/U = 0.5$.

VI. INHOMOGENEOUS SYSTEM: OPTICAL LATTICES IN AN EXTERNAL TRAPPING POTENTIAL

We extend the RPA formalism to real space and include a spatially inhomogeneous potential, which is taken into account in the BHM through a site-dependent chemical potential. The self consistent MF solution produces alternating shells of insulating and superfluid phases moving out from the center to the edge of the trap^{2,40,41}.

In the inhomogeneous system, the derivation of the equation for the Green's function is the same outlined in App. A, with the essential caution that the on-site energies ϵ_α^i and the tunneling coefficients $\hat{T}_{\alpha'\alpha\gamma\gamma'}^{ik}$ depends on position and must be calculated respectively for each site and for each pair of neighboring sites.

In the presence of an external trapping potential, the density and order parameter become non-uniform as shown in Fig. 11(a). With our specific choice of parameters, one finds a central Mott core at density $n = 1$, surrounded by a ring of superfluid. The sequence of panels (b) to (d) shows $G(\mathbf{r}, \mathbf{r}', \omega)$ as a function of \mathbf{r}' for fixed \mathbf{r} and ω , which roughly speaking represent the effect of perturbing the system at different points: perturbations in the SF regions produce a large effect all along the SF ring. As the perturbation moves to regions with lower order parameter near the SF-Mott interface its effect gets reduced and finally perturbations in Mott-like regions decrease exponentially and produce negligible effects.

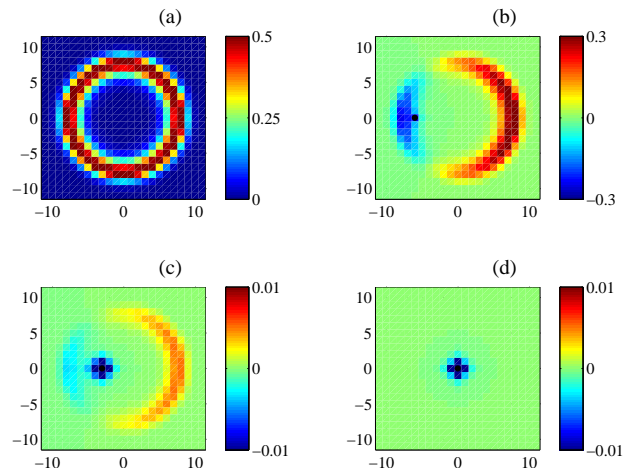


FIG. 11: (Color online) Inhomogeneous system: (a) order parameter in the trap: It is zero in the central MI core and finite and large in the surrounding SF ring. The other panels show $G(\mathbf{r}, \mathbf{r}')$ for a given value of the energy as a function of \mathbf{r}' for a fixed \mathbf{r} (black dot): (b) $\mathbf{r} = (-6, 0)$ in the SF ring; (c) $\mathbf{r} = (-3, 0)$ at the interface between the MI core and the SF ring; (d) $\mathbf{r} = (0, 0)$ in the center of the MI core.

The results shown in Fig. 11 are obtained for a given value of the energy ω . At different energies the structure remains the same, but the period of the oscillations along the ring changes. By integrating $G(\mathbf{r}, \mathbf{r}', \omega)$ over ω , one gets the equal-time correlation function $G(\mathbf{r}, \mathbf{r}')$. This quantity would maintain the ring-like behavior shown Fig. 11 and hence be qualitatively similar to the one calculated by Wessel and collaborators⁴².

Before searching for quantitative results in the non uniform system, one should ponder on the consequences of the problem in the normalization of the momentum distribution discussed in Sect. V, which might affect the extension of the RPA method to trapped systems. While this extension is technically simple, although it might become computationally quite expensive, its validity is to be questioned due to the co-existence in the same system of different phases (MI and SF), where, as we have explained above, RPA introduces different normalization factors. For this reason, while we believe one can get some insights on the correlations in the system, those pieces of information can be trusted only at the qualitative level.

VII. CONCLUDING REMARKS: RPA VS MEAN-FIELD

In this work, we have studied the excitations and the spatial correlations of the BHM in the RPA approximation. It is interesting to compare the information that is obtained between the mean field approximation and the RPA which includes a certain class of fluctuations:

- (1) The prediction of the SF to MI transition in the

$[\mu/U, t/U]$ plane calculated from the vanishing of the order parameter φ at the mean-field level and by the disappearance of the gapless excitation mode within RPA lead to exactly the same result for the boundaries of the insulating lobes.

(2) At the mean field level, one can extract information about the sound velocity using the compressibility-effective mass relation, while at the RPA level the sound velocity is given by the slope of the phonon mode. The two methods again lead to exactly the same result.

(3) The condensate fraction is $n_0 = |\varphi|^2$ at the mean-field level, whereas in the RPA treatment, it is extracted from the small q behavior of the spectral function and using the mean-field compressibility. Again the two methods lead to exactly the same result.

If the fluctuations around the mean field state were included self-consistently, they would renormalize the energy and order parameter. We then expect the SF state to be susceptible to fluctuations and the critical t/U to be shifted to a higher value than the one obtained by the MF theory.

The RPA method further gives information which is not included in the mean-field treatment. These include (i) the excitation spectra; (ii) their strengths; (iii) the existence of new gapped modes in the strongly interacting SF phase; (iv) the momentum distribution and spatial correlations in the system.

As an open question, we are left with the role of quantum fluctuations in the vicinity of the QPT, which as we discussed may have additional effects on physical quantities like the e.g. momentum distribution or the condensate fraction. As explained in App. C, it is to be expected that in our approach the momentum distribution is not normalized. In the Mott limit, a clear deviation from the normalization to the total number of atoms can be calculated analytically. Analogously, in the Bogoliubov regime, exactly recovered in RPA in the dilute limit, where one assumes $n = |\varphi|^2$, the normalization is larger than the total number of atoms once the depletion (given by the integral over all momenta different from zero of $|v_q|^2$) is added. However, while in the deep MI and SF regimes, the change in the normalization is just a small perturbation, close to the phase transition it is a striking effect. We attribute this to the fact that we perform RPA on the mean-field ground state, without taking the effect of RPA self-consistently into account. To this same reason, we attribute the existence of predictions (1) to (3) which are equal in the mean-field and RPA treatments.

Acknowledgments

C.M. acknowledges financial support by the EU through an EIF Marie-Curie Action. We thank R.B. Diener, P. Pedri, M. Randeria, and S. Stringari for helpful discussions.

APPENDIX A: GREEN'S FUNCTION FORMALISMS IN THE RPA APPROXIMATION

In this appendix we recall the main steps of the derivation of the Green's function formalism in the random phase approximation (RPA)^{26,27}.

RPA includes some fluctuations around the mean-field solution, which allows us to describe the excitations of the system. However, as explained in Sect. VII, these fluctuations are not included self consistently, allowing feedback into the mean field ground state. Also ignored are quantum fluctuations of the order parameter which are especially important close to the QPT (see also discussion in App. C).

Mean-field decoupling:

Substituting $a = \varphi + \tilde{a}$, $a^\dagger = \varphi + \tilde{a}^\dagger$, in Eq. (1), we obtain without any approximation

$$H = \sum_i \left[\frac{U}{2} n_i(n_i - 1) - \mu n_i - t\varphi(a_i^\dagger + a_i) + t\varphi^2 \right] + \frac{t}{2z} \sum_{\langle ij \rangle} (\tilde{a}_i^\dagger \tilde{a}_j + \tilde{a}_i \tilde{a}_j^\dagger). \quad (\text{A1})$$

The Hamiltonian H is thus rewritten as a sum of on-site Hamiltonians H_i^{MF} (indicated by the term in the square bracket which includes hopping at the mean field level), plus an inter-site hopping term, which is assumed to be small.

Random Phase Approximation:

In the basis given by the complete and orthonormal set of on-site eigenstates $|i\alpha\rangle$ of the on-site Hamiltonians H_i^{MF} , the Hamiltonian in Eq. (A1) takes the form

$$H = \sum_{i\alpha} \epsilon_{\alpha}^i L_{\alpha\alpha}^i - \frac{t}{2z} \sum_{\langle ij \rangle \alpha\alpha' \beta\beta'} \tilde{T}_{\alpha\alpha' \beta\beta'}^{ij} L_{\alpha\alpha'}^i L_{\beta\beta'}^j, \quad (\text{A2})$$

where we have defined

$$\begin{aligned} L_{\alpha\alpha'}^i &= |i\alpha\rangle\langle i\alpha'|, \\ \tilde{T}_{\alpha\alpha' \beta\beta'}^{ij} &\equiv \langle i\alpha|\tilde{a}_i^\dagger|i\alpha'\rangle\langle j\beta|\tilde{a}_j|j\beta'\rangle + \\ &\quad + \langle i\alpha|\tilde{a}_i|i\alpha'\rangle\langle j\beta|\tilde{a}_j^\dagger|j\beta'\rangle. \end{aligned} \quad (\text{A3})$$

For any pair of single particle operators A and B , the retarded ($\eta = +1$) or advanced ($\eta = -1$) Green's function, defined as

$$G_{r,a}(\tau) = -i\eta\theta(\eta\tau)\langle A(\tau)B(0) - B(0)A(\tau)\rangle, \quad (\text{A4})$$

can be written in the on-site eigenbasis as

$$G(\tau) = \sum_{\alpha\alpha' \beta\beta'} \langle i\alpha|A|i\alpha'\rangle\langle j\beta|B|j\beta\rangle G_{\alpha\alpha' \beta\beta'}^{ij}(\tau), \quad (\text{A5})$$

where $G_{\alpha\alpha'\beta\beta'}^{ij}(\tau) = \langle\langle L_{\alpha\alpha'}^i(\tau); L_{\beta\beta'}^j \rangle\rangle$.

In the energy domain, the Green's function is defined as

$$G(\omega) \equiv \langle\langle A; B \rangle\rangle_{\omega\pm} = \int_{-\infty}^{\infty} \frac{dt}{2\pi} G(\tau)_{r,a} e^{i\omega\pm\tau}. \quad (\text{A6})$$

A relation analogous to Eq. (A5) also holds for the energy resolved Green's functions.

In the uniform system at vanishing tunneling (deep Mott regime), $H = \sum_{i\alpha} \epsilon_{\alpha}^i L_{\alpha\alpha}^i$ is exactly diagonalized by the on-site eigenstates (Fock basis). The Green's function $G(\omega)$ can be calculated exactly to be

$$G_{MI}^{t=0}(\omega) = \frac{1}{2\pi} \left[\frac{n+1}{\omega - (E_{n+1} - E_n)} - \frac{n}{\omega + (E_{n-1} - E_n)} \right], \quad (\text{A7})$$

with $E_n = -\mu n + (U/2)n(n-1)$.

When the nearest neighbor tunneling plays a role, the commutator with the transition operators $L_{\alpha\alpha'}^i$ with the tunneling part of the Hamiltonian produces a coupling to three operators Green's functions. Following the prescriptions of RPA of replacing the average of a product with product of averages, one obtains

$$\begin{aligned} (E - \epsilon_{\alpha'}^i + \epsilon_{\alpha}^i) G_{\alpha\alpha'\beta\beta'}^{ij}(E) &= \\ &= \frac{1}{2\pi} (\langle L_{\alpha\alpha}^i \rangle - \langle L_{\alpha'\alpha'}^i \rangle) \delta_{\alpha\beta'} \delta_{\alpha'\beta} \delta_{ij} + \\ &- \frac{t}{z} (\langle L_{\alpha\alpha}^i \rangle - \langle L_{\alpha'\alpha'}^i \rangle) \sum_{\langle k \rangle i \gamma \gamma'} \tilde{T}_{\alpha'\alpha\gamma\gamma'}^{ik} G_{\gamma\gamma'\beta\beta'}^{kj}(E). \end{aligned} \quad (\text{A8})$$

At zero temperature results, $\langle L_{\alpha\alpha}^i \rangle$ are equal to 1 for the ground state and vanish otherwise.

For nearest-neighbor hopping and for a uniform system, where ϵ_{α}^i , $\langle L_{\alpha\alpha}^i \rangle$, and $\tilde{T}_{\alpha'\alpha\gamma\gamma'}^{ik}$ are site-independent (see Eq. (A3)), the same equation in momentum space takes the form

$$\begin{aligned} (E - \epsilon_{\alpha'} + \epsilon_{\alpha}) G_{\alpha\alpha'\beta\beta'}(E, \mathbf{q}) &= \\ &= \frac{1}{2\pi} (\langle L_{\alpha\alpha} \rangle - \langle L_{\alpha'\alpha'} \rangle) \delta_{\alpha\beta'} \delta_{\alpha'\beta} + \\ &+ \epsilon(\mathbf{q}) (\langle L_{\alpha\alpha} \rangle - \langle L_{\alpha'\alpha'} \rangle) \sum_{\gamma\gamma'} \tilde{T}_{\alpha'\alpha\gamma\gamma'} G_{\gamma\gamma'\beta\beta'}(E, \mathbf{q}). \end{aligned} \quad (\text{A9})$$

where $\epsilon(\mathbf{q}) = -(2t/z) \sum_i \cos(q_i)$, with i running over the dimensionality of the system and z being the number of nearest neighbors. In practice, for each value of the energy E and momentum \mathbf{q} , the solution of Eq. (A9) amounts to inverting a $2(N_s-1) \times 2(N_s-1)$ matrix, where N_s is the dimension of the number state basis considered.

The solution can also be found analytically to be¹⁶

$$G(\mathbf{q}, \omega) = \frac{1}{2\pi} \frac{\Pi(\mathbf{q}, \omega)}{1 - \epsilon(\mathbf{q})\Pi(\mathbf{q}, \omega)}, \quad (\text{A10})$$

where

$$\Pi(\mathbf{q}, \omega) = A_{11} + \frac{A_{12}A_{21}\epsilon(\mathbf{q})}{1 - \epsilon(\mathbf{q})A_{22}}, \quad (\text{A11})$$

$$A_{11} = \sum_{\alpha} \frac{y_{0\alpha} y_{\alpha 0}^{\dagger}}{\omega - \Delta_{\alpha}} - \frac{y_{0\alpha}^{\dagger} y_{\alpha 0}}{\omega + \Delta_{\alpha}}, \quad (\text{A12})$$

$$A_{22} = A_{11}^{\dagger}, \quad (\text{A13})$$

$$A_{12} = \sum_{\alpha} \frac{y_{0\alpha} y_{\alpha 0}}{\omega - \Delta_{\alpha}} - \frac{y_{0\alpha} y_{\alpha 0}}{\omega + \Delta_{\alpha}}, \quad (\text{A14})$$

$$A_{21} = A_{12}^{\dagger}, \quad (\text{A15})$$

with $|0\rangle$ indicating the ground state, $y_{\alpha 0}^{\dagger} = \langle \alpha | a^{\dagger} | 0 \rangle$ (and analogously the other terms), and $\Delta_{\alpha} = E_{\alpha} - E_0$. This equation can be easily evaluated numerically once the mean-field ground state wave function is known. This can be done analytically in the MI phase (see App. C), but has to be done numerically in the SF phase.

In principle, it is possible to apply this formalisms also in the non uniform case. One should then start from Eq. (A8) considering that both ϵ_{α}^i and $\tilde{T}_{\alpha'\alpha\gamma\gamma'}^{ik}$ generally depend on position. Hence, in that case, for each value of the energy the solution amounts to inverting a $2(N_s-1)N \times 2(N_s-1)N$ matrix, where N is the number of lattice wells considered.

APPENDIX B: BOGOLIUBOV THEORY FOR THE BHM

In this appendix we will present the details of the Bogoliubov treatment for the BHM. The results are expected to be valid in the weakly interacting SF regime, and were compared to the results of the RPA approximation in Sect. IV.

We start from the BHM

$$H = \sum_i \frac{U}{2} a_i^{\dagger} a_i^{\dagger} a_i a_i - \sum_i \mu n_i - \frac{t}{2z} \sum_{\langle ij \rangle} (a_i^{\dagger} a_j + a_i a_j^{\dagger}), \quad (\text{B1})$$

and define, as before, the fluctuation operators subtracting from the operators a and a^{\dagger} their mean-value

$$\tilde{a} = a - \varphi, \quad \tilde{a}^{\dagger} = a^{\dagger} - \varphi^*. \quad (\text{B2})$$

For a uniform system, one gets

$$\begin{aligned}
H = & \sum_i \left[\frac{U}{2} |\varphi|^4 - \mu |\varphi|^2 - t |\varphi|^2 \right] + \\
& + \sum_i \left[\tilde{a}_i^\dagger (U |\varphi|^2 - \mu - t) \varphi + h.c. \right] \\
& + \sum_i \left[\frac{U}{2} \left(\varphi^2 \tilde{a}_i^{\dagger 2} + 4 |\varphi|^2 \tilde{a}_i^\dagger \tilde{a}_i + \varphi^{*2} \tilde{a}_i^2 \right) + \right. \\
& \quad \left. - \mu \tilde{a}_i^\dagger \tilde{a}_i - \frac{t}{2z} \sum_{\langle j \rangle_i} \left(\tilde{a}_i^\dagger \tilde{a}_j + \tilde{a}_j^\dagger \tilde{a}_i \right) \right] + \\
& + \text{3rd} + \text{4th order in } \tilde{a} \text{ and } \tilde{a}^\dagger.
\end{aligned} \tag{B3}$$

To minimize the energy one has to set to zero the first order, leading to the discretized version of the Gross-Pitaevskii equation for the uniform system

$$U |\varphi|^2 - \mu - t = 0 \implies \varphi_{GP} = \sqrt{\frac{\mu + t}{U}}. \tag{B4}$$

The quantity $|\varphi|^2$ is the density in the uniform system, and is related to the chemical potential. Conversely, for a given density $|\varphi|^2$, the chemical potential is given by

$$\mu = U |\varphi|^2 - t, \tag{B5}$$

namely the kinetic energy plus interaction energy. Strictly speaking the kinetic energy of the condensate is zero, and t is just a shift due to the choice of the zero of energy. This approach does not include any phase transition, because the SF fraction $|\varphi|^2$ is always equal to the total density.

To diagonalize the second order terms in the Hamiltonian (H_2), we perform a transformation to momentum space

$$\tilde{a}_i = \frac{1}{N} \sum_{\mathbf{q}} e^{-i\mathbf{q} \cdot \mathbf{r}_i} \tilde{a}_{\mathbf{q}}, \tag{B6}$$

$$\tilde{a}_i^\dagger = \frac{1}{N} \sum_{\mathbf{q}} e^{i\mathbf{q} \cdot \mathbf{r}_i} \tilde{a}_{\mathbf{q}}^\dagger, \tag{B7}$$

so that, finally it reads

$$\begin{aligned}
H_2 = & -\frac{1}{2} \sum_{\mathbf{q}} [2U |\varphi|^2 - \mu + \epsilon(\mathbf{q})] + \\
& + \frac{1}{2} \sum_{\mathbf{q}} \left[(2U |\varphi|^2 - \mu + \epsilon(\mathbf{q})) \left(\tilde{a}_{\mathbf{q}}^\dagger \tilde{a}_{\mathbf{q}} + \tilde{a}_{-\mathbf{q}} \tilde{a}_{-\mathbf{q}}^\dagger \right) + \right. \\
& \quad \left. + U \varphi^2 \tilde{a}_{\mathbf{q}}^\dagger \tilde{a}_{-\mathbf{q}}^\dagger + U \varphi^{*2} \tilde{a}_{-\mathbf{q}} \tilde{a}_{\mathbf{q}} \right],
\end{aligned} \tag{B8}$$

where, as before, $\epsilon(\mathbf{q}) = -(2t/z) \sum_i \cos(q_i)$. Then, we apply the Bogoliubov transformation which diagonalizes H_2

$$\begin{pmatrix} \tilde{a}_{\mathbf{q}} \\ \tilde{a}_{-\mathbf{q}}^\dagger \end{pmatrix} = \begin{pmatrix} u_{\mathbf{q}} b_{\mathbf{q}} + v_{-\mathbf{q}}^* b_{-\mathbf{q}}^\dagger \\ u_{-\mathbf{q}}^* b_{-\mathbf{q}}^\dagger + v_{\mathbf{q}} b_{\mathbf{q}} \end{pmatrix}, \tag{B9}$$

with the additional condition $|u_{\mathbf{q}}|^2 - |v_{-\mathbf{q}}|^2 = 1$ to preserve the commutation relations. This is equivalent to the Bogoliubov equations

$$\begin{aligned}
(\mathcal{L}_{\mathbf{q}} - \hbar\omega_{\mathbf{q}}) u_{\mathbf{q}} + U \varphi^2 v_{\mathbf{q}} &= 0, \\
(\mathcal{L}_{\mathbf{q}} + \hbar\omega_{\mathbf{q}}) v_{\mathbf{q}} + U \varphi^{*2} u_{\mathbf{q}} &= 0,
\end{aligned}$$

where $\mathcal{L}_{\mathbf{q}} = U |\varphi|^2 + (4t/z) \sum_i \sin^2(q_i d/2)$.

The solution for the Bogoliubov spectrum and the Bogoliubov amplitudes is given by

$$\hbar\omega_{\mathbf{q}} = \sqrt{\frac{4t}{z} \sum_i \sin^2\left(\frac{q_i}{2}\right) \left[\frac{4t}{z} \sum_i \sin^2\left(\frac{q_i}{2}\right) + 2U |\varphi|^2 \right]}, \tag{B10}$$

$$u_{\mathbf{q}} + v_{\mathbf{q}} = \sqrt{\frac{\mathcal{L}_{\mathbf{q}} - U \varphi^2}{\hbar\omega_{\mathbf{q}}}} = \sqrt{\frac{(4t/z) \sum_i \sin^2(q_i/2)}{\hbar\omega_{\mathbf{q}}}}, \tag{B11}$$

$$u_{\mathbf{q}} - v_{\mathbf{q}} = \sqrt{\frac{\hbar\omega_{\mathbf{q}}}{\mathcal{L}_{\mathbf{q}} - U \varphi^2}} = \sqrt{\frac{\hbar\omega_{\mathbf{q}}}{(4t/z) \sum_i \sin^2(q_i/2)}}. \tag{B12}$$

For $\mathbf{q} \rightarrow 0$, the spectrum shows a linear behavior in $|\mathbf{q}|$, $\hbar\omega_{\mathbf{q}} \approx |\mathbf{q}| \sqrt{(2t/z) U |\varphi|^2}$ with sound velocity $c = \sqrt{(2t/z) U |\varphi|^2}$.

In the Bogoliubov theory the momentum distribution is given by

$$n(\mathbf{q}) = |\varphi|^2 \delta_{\mathbf{q},0} + |v_{-\mathbf{q}}|^2. \tag{B13}$$

It is evident that starting from the fact that $|\varphi|^2$ equals the total density in the uniform system, the integral of the momentum distribution $\int n(\mathbf{q}) d\mathbf{q}$ will exceed this value by the depletion $n_D = \int |v(\mathbf{q})|^2 d\mathbf{q}$. In the limit of validity of the Bogoliubov approach, this quantity is very small.

APPENDIX C: ANALYTIC CALCULATION OF THE MOMENTUM DISTRIBUTION IN THE MOTT REGIME IN THE RPA APPROXIMATION

In the RPA approximation, the momentum distribution in the MI regime can be calculated analytically. In this appendix, we will present the results for 1, 2, and 3D systems, with the aim of pointing out that close to the phase transition quantum fluctuation play a major role and are not correctly taken into account by RPA.

In the MI regime, the RPA Green's function in Eq. (A10) can be written as

$$G_{MI}(\mathbf{q}, \omega) = \frac{1}{2\pi} \frac{A_{11}(\omega)}{1 - \epsilon(\mathbf{q})A_{11}(\omega)}, \quad (C1)$$

where A_{11} has been defined in Eq. (A12), $A_{12} = A_{21} = 0$ in the MI, and $\epsilon(\mathbf{q}) = -(2t/z) \sum_i \cos(q_i)$ as before.

In particular for the MI at density n (i.e. where the on-site ground state is $|0\rangle = |n\rangle$), we get

$$A_{11}(\omega) = \frac{n+1}{\omega - (E_{n+1} - E_n)} - \frac{n}{\omega + (E_{n-1} - E_n)}, \quad (C2)$$

(with $E_n = -n\mu + (U/2)n(n-1)$) which obviously coincides a part from a factor $1/2\pi$ with the Green's function for the MI at zero tunneling previously introduced in Eq. (A7).

By using definitions in Eqs. (C1,C2) above and defining $\Delta_{\pm} = E_{n\pm 1} - E_n$, it is straightforward to see that the Green's function takes the form

$$G_{MI} = \frac{1}{2\pi} \frac{(n+1)(\omega + \Delta_-) - n(\omega - \Delta_+)}{(\omega - \Delta_+)(\omega + \Delta_-) - \epsilon(\mathbf{q})[n\omega + (n+2)\Delta_-]}, \quad (C3)$$

whose poles ω_{\pm} can be calculated analytically and have a momentum dependence due to the kinetic energy $\epsilon(\mathbf{q})$ in Eq. (C1). Hence, the Green's function close to the poles ($\omega \approx \omega_{\pm}$), is approximately

$$G_{MI} \approx \frac{1}{2\pi} \frac{(n+1)(\omega_{\pm} + \Delta_-) - n(\omega_{\pm} - \Delta_+)}{(\omega_{\pm} - \omega_{\mp})(\omega - \omega_{\pm})}. \quad (C4)$$

Consequently, the momentum distribution reads

$$n(\mathbf{q}) = -\frac{(n+1)(\omega_- + \Delta_-) - n(\omega_- - \Delta_+)}{\omega_- - \omega_+}. \quad (C5)$$

In the deep MI ($t = 0$), $\omega_{\pm} = \pm\Delta_{\pm}$ and the momentum distribution is simply given by $n(\mathbf{q}) = n$, which integrated over the allowed momenta (equal to the total

number of wells) gives the total number of atoms. At finite tunneling, the kinetic energy $\epsilon(\mathbf{q})$ gives a modulation to the momentum distribution.

To find the normalization of $n(\mathbf{q})$, we integrate numerically the analytic expression in Eq. (C5) for different dimensions. The result is shown in Fig. 12 for the MI with $n = 1$, and clearly shows an increase of the normalization toward the phase transition. We attribute this effect to the fact that quantum fluctuations are not completely taken into account in this approach. This interpretation is confirmed by the fact that this effect diminishes by increasing the dimensionality of the system.

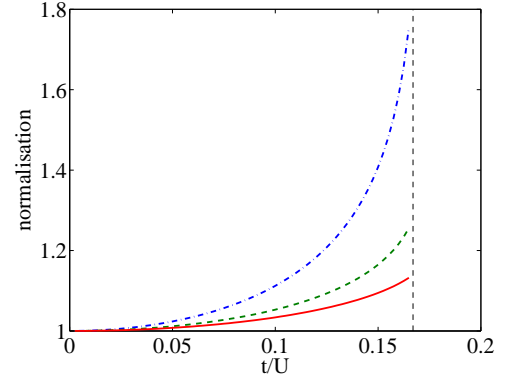


FIG. 12: Normalization of $n(q)$ for $\mu/U = 0.5$ as a function of t/U in dimensions 1D (blue dashed-dotted line), 2D (green dashed line) and 3D (red full line). The thin vertical line indicates the phase transition.

It is interesting to note that while the normalization of the momentum distribution is violated, the sum-rule is perfectly satisfied. The strengths at positive and negative energy are respectively given by

$$S_{\pm} = \frac{(n+1)(\omega_{\pm} + \Delta_-) - n(\omega_{\pm} - \Delta_+)}{\omega_{\pm} - \omega_{\mp}}, \quad (C6)$$

such that $S_+ + S_- = 1$.

¹ I. Bloch, Nature Phys. **1**, 23 (2005).

² D. Jaksch, C. Bruder, J.I. Cirac, C.W. Gardiner, and P. Zoller, Phys. Rev. Lett. **81**, 3108 (1998).

³ M. Greiner, O. Mandel, T. Esslinger, T.W. Hänsch, I. Bloch, Nature **415**, 39 (2002).

⁴ M. P. A. Fisher, P. B. Weichman, G. Grinstein, and D. S. Fisher, Phys. Rev. B **40**, 546 (1989).

⁵ S. Sachdev, *Quantum Phase Transitions*, Cambridge University Press, London, 1999.

⁶ J.E. Mooij, B.J. van Wees, L.I. Geerligs, M. Peters, R. Fazio, and G. Schön, Phys. Rev. Lett. **65** 645 (1990).

⁷ B.C. Crooker, B. Hebral, E.N. Smith, Y. Takano,

and J.D. Reppy, Phys. Rev. Lett. **51**, 666 (1983); M.H.W. Chan, K.I. Blum, S.Q. Murphy, G.K.S. Wong, and J.D. Reppy, Phys. Rev. Lett. **61**, 1950 (1988).

⁸ M.P.A. Fisher and D.H. Lee, Phys. Rev. B **39**, 2756 (1989); D.R. Nelson and H.S. Seung, Phys. Rev. B **39** 9153 (1989).

⁹ A. Auerbach, *Interacting Electrons and Quantum Magnetism*, Springer-Verlag (New York, 1994).

¹⁰ E. Altman and A. Auerbach, Phys. Rev. Lett. **89**, 250404 (2002).

¹¹ T. Stöferle, H. Moritz, C. Schori, M. Köhl, and T. Esslinger, Phys. Rev. Lett. **92**, 130403 (2004).

¹² M. Krämer, C. Tozzo, and F. Dalfovo, Phys. Rev. A **71**,

- 061602(R) (2005).
- ¹³ D. van Oosten, D.B.M. Dickerscheid, B. Farid, P. van der Straten, and H.T.C. Stoof, Phys. Rev. A **71**, 021601(R) (2005).
 - ¹⁴ K. Sengupta and N. Dupuis, Phys. Rev. A **71**, 033629 (2005).
 - ¹⁵ S. Konabe, T. Nikuni, M. Nakamura, Phys. Rev. A **73**, 033621 (2006).
 - ¹⁶ Y. Ohashi, M. Kitaura, and H. Matsumoto, Phys. Rev. A **73**, 033617 (2006).
 - ¹⁷ S.D. Huber, E. Altman, H.P. Büchler, and G. Blatter, Phys. Rev. B **75**, 085106 (2007).
 - ¹⁸ R. Grimm, *Ultracold Fermi gases in the BEC-BCS crossover: a review from the Innsbruck perspective*, in “Ultracold Fermi Gases”, Proceedings of the International School of Physics “Enrico Fermi”, Course CLXIV, Varenna, 20 - 30 June 2006, edited by M. Inguscio, W. Ketterle, and C. Salomon.
 - ¹⁹ M. Greiner, O. Mandel, T.W. Hänsch, and I. Bloch, Nature **419**, 51 (2002).
 - ²⁰ J. Zakrzewski, Phys. Rev. A **71**, 043601 (2005).
 - ²¹ K. Sheshadri, H.R. Krishnamurthy, R. Pandit, and T.V. Ramakrishnan, Europhys. Lett. **22**, 257 (1993).
 - ²² J.K. Freericks and H. Monien, Europhys. Lett. **26**, 545 (1994); Phys. Rev. B **53**, 2691 (1996).
 - ²³ D.S. Rokhsar and B.G. Kotliar, Phys. Rev. B **44**, 10328 (1991); J.J. Garcia-Ripoll, J.I. Cirac, P. Zoller, C. Kollath, U. Schollwöck, and J. von Delft, Optics Express **12**, 42 (2004).
 - ²⁴ G.G. Batrouni, R.T. Scalettar, and G.T. Zimanyi, Phys. Rev. Lett. **65**, 1765 (1990).
 - ²⁵ W. Krauth and N. Trivedi, Europhys. Lett. **14**, 627 (1991).
 - ²⁶ S.B. Haley and P. Erdős, Phys. Rev. B **5**, 1106 (1972).
 - ²⁷ D.N. Zubarev, Soviet Physics Uspekhi **3**, 320 (1960).
 - ²⁸ C. Schroll, F. Marquardt, and C. Bruder, Phys. Rev. A **70**, 053609 (2004).
 - ²⁹ F. Gerbier, A. Widera, S. Fölling, O. Mandel, T. Gericke, and I. Bloch, Phys. Rev. Lett. **95**, 050404 (2005); Phys. Rev. A **72**, 053606 (2005).
 - ³⁰ D.M. Gangardt, P. Pedri, L. Santos, and G.V. Shlyapnikov, Phys. Rev. Lett. **96**, 040403 (2006).
 - ³¹ I.B. Spielman, W.D. Phillips, and J.V. Porto, Phys. Rev. Lett. **98**, 080404 (2007).
 - ³² R.B. Diener, Q. Zhou, H. Zhai, T.-L. Ho, Phys. Rev. Lett. **98**, 180404 (2007).
 - ³³ A. Griffin, *Excitations in a Bose-Condensed Liquid*, (Cambridge, 1993).
 - ³⁴ L. Pitaevskii and S. Stringari, *Bose-Einstein Condensation*, (Oxford University Press, Oxford, 2003).
 - ³⁵ The one-dimensionality of the system considered in the calculations presented here justifies the diverging behaviour of the DOS at small energies.
 - ³⁶ E. Taylor and E. Zaremba, Phys. Rev. A **68**, 053611 (2003).
 - ³⁷ M. Krämer, C. Menotti, L. Pitaevskii and S. Stringari, Eur. Phys. J. D **27**, 247 (2003).
 - ³⁸ C. Menotti, M. Kraemer, A. Smerzi, L. Pitaevskii, and S. Stringari, Phys. Rev. A **70**, 023609 (2004).
 - ³⁹ R.B. Diener, R. Sensarma, and M. Randeria, cond-mat/arXiv:0709.2653v1.
 - ⁴⁰ G.G. Batrouni, V. Rousseau, R.T. Scalettar, M. Rigol, A. Muramatsu, P.J.H. Denteneer, and M. Troyer, Phys. Rev. Lett. **89**, 117203 (2002).
 - ⁴¹ S. Fölling, A. Widera, T. Müller, F. Gerbier, and I. Bloch, Phys. Rev. Lett. **97**, 060403 (2006).
 - ⁴² S. Wessel, F. Alet, M. Troyer, G.G. Batrouni, Phys. Rev. A **70**, 053615 (2004).